LETTER

doi:10.1038/nature21362

C. elegans neurons jettison protein aggregates and mitochondria under neurotoxic stress

Ilija Melentijevic[1], Marton L. Toth[1]*, Meghan L. Arnold[1]*, Ryan J. Guasp[1], Girish Harinath[1], Ken C. Nguyen[2], Daniel Taub[3,4], J. Alex Parker[5], Christian Neri[6], Christopher V. Gabel[3,4], David H. Hall[2] & Monica Driscoll[1]

The toxicity of misfolded proteins and mitochondrial dysfunction are pivotal factors that promote age-associated functional neuronal decline and neurodegenerative disease[1,2]. Accordingly, neurons invest considerable cellular resources in chaperones, protein degradation, autophagy and mitophagy to maintain proteostasis and mitochondrial quality[3,4]. Complicating the challenges of neuroprotection, misfolded human disease proteins and mitochondria can move into neighbouring cells via unknown mechanisms, which may promote pathological spread[5,6]. Here we show that adult neurons from *Caenorhabditis elegans* extrude large (approximately 4 μm) membrane-surrounded vesicles called exophers that can contain protein aggregates and organelles. Inhibition of chaperone expression, autophagy or the proteasome, in addition to compromising mitochondrial quality, enhances the production of exophers. Proteotoxically stressed neurons that generate exophers subsequently function better than similarly stressed neurons that did not produce exophers. The extruded exopher transits through surrounding tissue in which some contents appear degraded, but some non-degradable materials can subsequently be found in more remote cells, suggesting secondary release. Our observations suggest that exopher-genesis is a potential response to rid cells of neurotoxic components when proteostasis and organelle function are challenged. We propose that exophers are components of a conserved mechanism that constitutes a fundamental, but formerly unrecognized, branch of neuronal proteostasis and mitochondrial quality control, which, when dysfunctional or diminished with age, might actively contribute to pathogenesis in human neurodegenerative disease and brain ageing.

While studying age-associated dendritic restructuring in *C. elegans* neurons[7], we noticed that fluorescent signals originating from neurons sometimes appeared situated outside of the cell in defined vesicle-like structures that we call exophers (Fig. 1a–c, Extended Data Figs 1a–c, 2g). We first characterized exophers associated with the six gentle touch receptor neurons, for which cell bodies and dendrites are easily visualized. We found that exophers are comparable in size (average diameter 3.8 μM) to neuronal somas (Extended Data Fig. 1d). The size of the vesicles, the morphological stages in their biogenesis (Fig. 1a–c), and the genetic requirements for their production (Extended Data Table 1a) distinguish them from much smaller exosomes (around 30–100 nm; Extended Data Table 2 compares exophers to characterized extracellular vesicles). Neuronal exophers do not seem to result from classical cell division: (1) exophers did not stain with the nuclear DNA indicator DAPI (Fig. 1b); (2) cell division-inhibiting hydroxyurea[8] did not change exopher levels ($n > 30$ per trial, three trials); and (3) RNA interference (RNAi)-mediated disruption of cell cycle genes did not change exopher detection (Extended Data Table 1b).

We found that exopher production is not restricted to a specific transgene reporter or line (examples in Fig. 1, Extended Data Fig. 1). Amphid neurons that are dye-filled via openings to the outside environment[9] (Extended Data Fig. 1e, f) can produce exophers, confirming that exophers can form under native physiological cellular conditions. Exopher production differs markedly among the six touch receptor neurons, with ALMR neurons producing exophers most frequently (Fig. 1d). Many neuronal types can produce exophers, including dopaminergic PDE and CEP neurons (Extended Data Fig. 1g, h), FLP neurons (not shown) and sensory ASER neurons (Extended Data Fig. 1i).

Time-lapse analyses (Supplementary Videos 1, 2) revealed that exophers typically arise from the soma by asymmetrically amassing labelled protein to create a balloon-like extrusion via a pinching off event; the exopher compartment then moves outward from the neuronal cell body (extrusion approximately 15–100 min; Fig. 1a, Extended Data Fig. 1a). The plasma membrane reporter $P_{mec\text{-}4}$PH(plcDelta)::GFP (Extended Data Fig. 2a) and electron microscopy data (Extended Data Fig. 2) confirm that exophers are membrane-bound. Exophers can initially remain connected to the soma by a thin thread-like tube (Fig. 1c) that allows the transfer of tagged proteins and calcium into the attached exopher compartment (Extended Data Figs 1a, 3, Supplementary Video 2). Exophers ultimately disconnect from the originating neuronal soma (Extended Data Fig. 3).

Time-lapse studies indicated that aggregating mCherry often appeared preferentially concentrated into exophers, and neurons expressing the huntingtin (Htt) protein with a neurotoxic polyglutamine tract of 128 repeats (Htt-Q128) could also concentrate and extrude this aggregating protein in exophers (Fig. 2a, b). We therefore further queried the relationship of aggregating or toxic protein expression to exopher production. Strains expressing Q128 (toxic, with high levels of apparent aggregation[10,11]) produced significantly more exophers than strains that did not express polyQ or that expressed Htt-Q19 (non-toxic and low aggregation) (Fig. 2c). Likewise, aggregating mCherry lines exhibited higher average exopher numbers over adult life than lines expressing soluble green fluorescent protein (GFP) (see Fig. 2d). High aggregate load in individual neurons was predictive of increased exopher production on the following day (Fig. 2e). Conversely, mCherry RNAi reduced the number of exophers by approximately one-half in a line producing aggregating mCherry (Fig. 2f). Although our studies cannot determine the relative contribution of aggregate load from protein expression levels, they suggest that proteostatic challenges increase exopher production. Consistent with a potential role for exophers in the elimination of potentially harmful neuronal contents, the expression of amyloid-forming human Alzheimer's disease fragment amyloid-β_{1-42} in ASER neurons increases exopher numbers (Fig. 2g). Our combined observations on exopher formation, contents and frequency of detection suggest that exophers

[1]Department of Molecular Biology and Biochemistry, Nelson Biological Laboratories, Rutgers, The State University of New Jersey, Piscataway, New Jersey 08854, USA. [2]Department of Neuroscience, Albert Einstein College of Medicine, Bronx, New York 10461, USA. [3]Department of Physiology and Biophysics, Boston University School of Medicine, Boston, Massachusetts 02118, USA. [4]Boston University Photonics Center, Boston, Massachusetts 02215, USA. [5]Département de Neurosciences, Université de Montréal CRCHUM, Montréal H2X 0A9, Canada. [6]CNRS, UMR 8256, Brain-C team, Paris, France, and Sorbonnes Universités, University Pierre and Marie Curie (UPMC) Univ Paris 06, Paris, France.
*These authors contributed equally to this work.

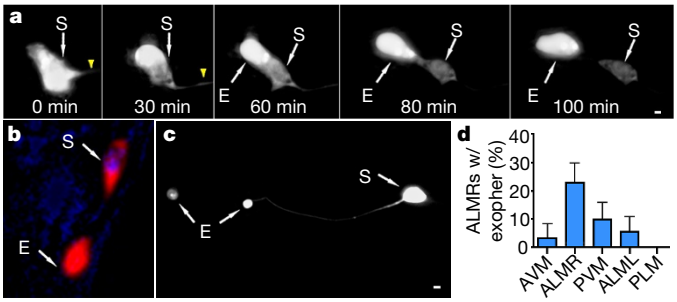

Figure 1 | *C. elegans* touch neurons can extrude cytoplasmic contents. **a**, An exopher is generated with a notable concentration of fluorescent protein segregated to the extrusion. Strain is Is[$P_{mec\text{-}4}$mCh2]. Shown is an ALM neuron with mCherry-visualized cytoplasm and aggregates. Arrowheads denote neuronal process. See Supplementary Video 1. **b**, Exophers do not include nuclear-like levels of DNA. Blue, DAPI; red, cytoplasm. 0 out of 25 exophers but 25 out of 25 soma were DAPI positive. Strain is Is[$P_{mec\text{-}4}$mCh2]. **c**, An ALMR soma with one attached (right) and one unattached (left) exopher. Strain is Is[$P_{mec\text{-}4}$mCh1]; Is[$P_{mec\text{-}4}$GFP]. **d**, Individual touch neurons differ in their production of detectable exophers. ALMR neurons produce the most (approximately 23%) for Is[$P_{mec\text{-}18}$*sid-1*]; Is[$P_{mec\text{-}4}$mCh3], and PLM neurons fail to generate detectable extrusions (0 out of >500). 12 trials of RNAi empty vector controls with $n > 500$ total for each neuron. All animals are adult day 2. E, exophers; S, soma. Scale bars, 2 μm. Data in **d** are mean ± s.d.

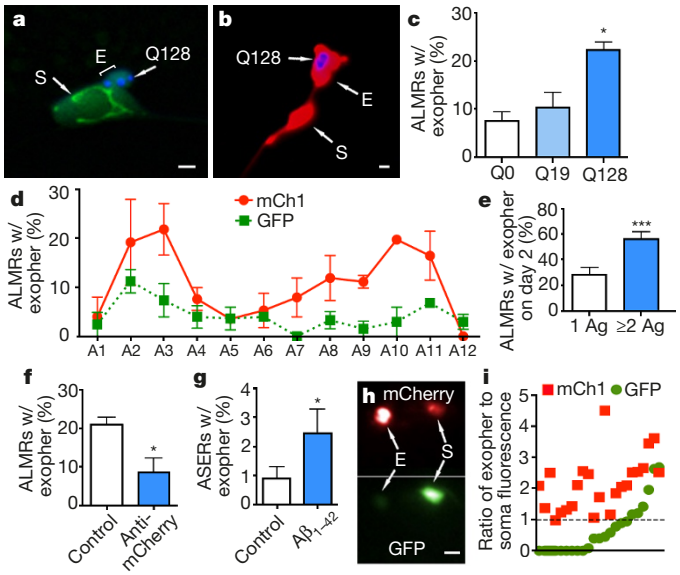

Figure 2 | Touch neurons under proteotoxic stress jettison aggregation-prone proteins into exophers. **a**, CFP-tagged Q128 (blue) concentrated into a budding domain. Green, mitochondria GFP signal. **b**, Mature exopher containing Q128–CFP aggregates. Five out of ten ALM exophers were Q128–CFP positive. These five had no detectable Q128–CFP in their somas. Strain in **a** and **b** is Is[$P_{mec\text{-}4}$mCh2; $P_{mec\text{-}3}$Q128CFP]. **c**, Neurons expressing Q128–CFP produce more exophers than neurons expressing Q19–CFP. Strains are Is[$P_{mec\text{-}4}$GFP] (Q0), Is[$P_{mec\text{-}7}$YFP; $P_{mec\text{-}3}$Q19CFP] (Q19), and Is[$P_{mec\text{-}7}$YFP; $P_{mec\text{-}3}$Q128CFP] (Q128). $n > 100$ total for each strain, 3 trials; polyQ-expressing strains have similar expression levels[10]. **d**, Touch neuron exophers are detectable in young adults, diminish in abundance in midlife, and increase again in older animals. Longitudinal study of Is[$P_{mec\text{-}4}$GFP] and Is[$P_{mec\text{-}4}$mCh1] (starting $n = 75$ total per strain), 3 trials, adult days A1–A12. $P < 0.001$, variation between days and strains. A similar early adulthood peak occurs in dye-filled amphid neurons (Extended Data Fig. 1f) and in the *hsf-1* mutant (Extended Data Fig. 1j). **e**, Multiple early visible aggregates predict later exopher formation. On adult day 1, animals were segregated by number of mCherry aggregates (1 aggregate (Ag) versus ≥ 2 Ag) in the ALMR soma, and scored for exophers on adult day 2. $n > 130$ total per condition, 5 trials. Strain is Is[$P_{mec\text{-}4}$mCh1]. **f**, Reducing mCherry expression levels using an anti-mCherry RNAi reduces exopher levels. Strain is Is[$P_{mec\text{-}18}$*sid-1*]; Is[$P_{mec\text{-}4}$mCh3], $n > 35$ per trial, 3 trials. **g**, ASER neurons expressing human toxic amyloid-β protein fragment exhibit increased exopher production. Adult day 2, 7 trials, $n > 800$ total for each strain, *sesIs2512*[$P_{gcy\text{-}5}$GFP], and *sesIs25*[$P_{flp\text{-}6}$Aβ$_{1\text{-}42}$; $P_{gcy\text{-}5}$GFP]. **h**, **i**, Aggregation-prone mCherry is preferentially segregated into the exopher compared to non-aggregating GFP, which is more concentrated in the soma. **h**, mCherry (top) and GFP (bottom) channels from an ALMR exopher and soma pair in a strain co-expressing Is[$P_{mec\text{-}4}$mCh1] and Is[$P_{mec\text{-}4}$GFP]. **i**, Quantification of mCherry and GFP fluorescence ratios for exopher and soma pairs. Each point represents an exopher-to-soma fluorescence ratio for either GFP or mCherry. Each cell has a paired GFP and mCherry E/S ratio, aligned vertically, $n = 23$ pairs. Mean E/S ratios of mCherry and GFP were 2.2 and 0.75, respectively. All animals, adult day 2. Scale bars, 2 μm. Data are mean ± s.e.m. $^*P < 0.05$, $^{***}P < 0.001$, unpaired *t*-test (**e**, **f**, **g**), one-way ANOVA (**d**) and one-way ANOVA with Tukey's test (**c**).

preferentially include aggregated, excess, or otherwise neurotoxic proteins for removal.

To address the hypothesis that aggregation-prone proteins might be selectively extruded in exophers, we constructed a line that expressed both an aggregation-prone mCherry (Is[$P_{mec\text{-}4}$mCh1]) and a non-aggregating GFP (Is[$P_{mec\text{-}4}$GFP]) and compared the red and green fluorescence distribution between exophers and somas (example in Fig. 2h, data in Fig. 2i). In 22 out of 23 exophers, we found higher relative levels of mCherry in the exopher, and higher relative levels of GFP in the soma. Neurons appear to extrude aggregation-prone mCherry preferentially compared with soluble GFP, suggesting that deleterious materials are identified and sorted for export during exopher-genesis.

To investigate whether proteostatic challenges enhance the exopher production response, we manipulated the *in vivo* protein-folding milieu. We found a roughly sixfold increase in exopher production in an *hsf-1(sy441)* mutant deficient in the core proteostasis transcription factor HSF-1 (and therefore deficient in chaperone expression) (Fig. 3a). We impaired autophagy by treating animals with the pharmacological inhibitor spautin-1 and by RNAi knockdown (*lgg-1*, *atg-7*, *bec-1*, *lgg-1/2*) in a strain expressing aggregation-prone mCherry, and measured a significant increase in exopher incidence (Fig. 3b, c). Impairment of proteasome activity with the inhibitor MG132 on strain Is[$P_{mec\text{-}4}$mCh1] also increased exopher production (Fig. 3d). Given that inhibiting several facets of proteostasis increases exopher extrusion, we suggest that exophers may constitute a previously undescribed component of the proteostasis network, which may function as a backup or alternative response to rid cells of neurotoxic aggregates/proteins when proteostasis becomes overwhelmed by mounting intracellular proteotoxicity.

Exopher production occurs with a notable bimodal distribution throughout adult life: exophers are most commonly observed at adult days A2–A3, diminish in abundance at A4–A8, and then reappear again later in life at approximately A10–A11 (Fig. 2d; similar young adult pattern with dye-filled amphid neurons, Extended Data Fig. 1f; and with a 1-day earlier onset in an *hsf-1* mutant, Extended Data Fig. 1j). The distinctive temporal production profile suggests that conditions permissive for exopher production exist in young adulthood but can then be limited or remain below a threshold until late adulthood. The coincidence of the early peak with a transition in *C. elegans* young adult proteostasis management[12–14] suggests that the first wave of exopher-genesis may serve as a normal component of an orchestrated proteostasis reset in young adulthood that involves the removal of neuronal debris generated during development; the later adult increase in exopher production may be the consequence of age-associated decline in proteostatic robustness.

Rather than inducing neuronal death or dysfunction, exopher-genesis seems to be beneficial. First, in hundreds of longitudinal observations, we did not observe neuronal loss after exopher production: exophers are distinct from apoptotic bodies in their biogenesis (Fig. 1a, Extended Data Fig. 1a), and the soma of an exopher-producing neuron retains normal ultrastructural features (Extended Data Fig. 2e).

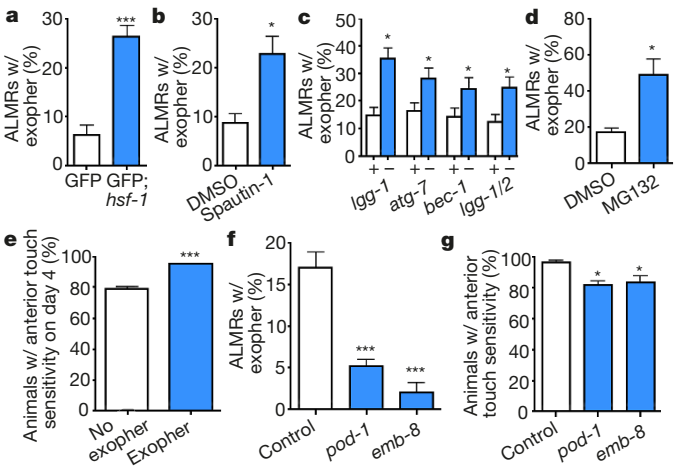

Figure 3 | Disruption of multiple branches of proteostasis increases exopher formation. a, Disrupting proteostasis by *hsf-1* impairment increases exopher formation. Strains were Is[$P_{mec\text{-}4}$GFP] and Is[$P_{mec\text{-}4}$GFP]; *hsf-1(sy441)* (GFP and GFP; *hsf-1*, respectively), $n > 280$ total per strain. **b**, Pharmacological inhibition of autophagy by spautin-1 increases the occurrence of exophers. Strain is Is[$P_{mec\text{-}4}$GFP], $n > 80$ total per condition. **c**, RNAi knockdown (blue) of autophagy genes *lgg-1*, *atg-7* and *bec-1* increases the occurrence of exophers. Strain is Is[$P_{mec\text{-}18}$*sid-1*]; Is[$P_{mec\text{-}4}$mCh3]. White, empty vector control. *lgg-1* (5 trials), *atg-7* (5 trials), *bec-1* (4 trials) and *lgg-1/2* (5 trials), $n > 100$ total per condition. **d**, Pharmacological inhibition of the proteasome by MG132 treatment increases the occurrence of exophers. Strain is Is[$P_{mec\text{-}4}$mCh1], 3 trials, $n > 33$ per trial. **e**, Q128-expressing animals with an ALMR exopher on day 2 have better anterior touch sensitivity on adult day 4 compared to animals with no apparent early exopher. Strain is Is[$P_{mec\text{-}4}$mCh2; $P_{mec\text{-}3}$Q128CFP], which exhibits accelerated functional decline of touch neurons. $n > 100$ animals total, 3 trials. Note that differences are likely to be underestimated as the 'no exopher' category should include animals that have produced exophers but were not present at the time of sampling. **f**, RNAi knockdown of *pod-1* or *emb-8* significantly decreases exopher detection, defining a genetic approach to limiting exopher-genesis. Strain is Is[$P_{mec\text{-}18}$*sid-1* $P_{mec\text{-}4}$mCh3]. $n > 100$ total per condition, 4 trials. **g**, RNAi knockdown of *pod-1* and *emb-8* is associated with a decrease in anterior touch sensitivity in day 4 adults. Strain is Is[$P_{mec\text{-}18}$*sid-1* $P_{mec\text{-}4}$mCh3], an aggregation-prone mCherry line which, like wild type, maintains strong touch sensitivity in young adult life. *pod-1* and *emb-8* RNAi knockdown from egg-lay had no effect on young animal touch sensitivity, but L4-adult *pod-1* and *emb-8* RNAi knockdown reduced exopher production and decreased touch sensitivity in day 4 adults. $n > 130$ total per condition, 3 trials. All animals, adult day 2. Scale bars, 2 μm. Data are mean ± s.e.m. (**a**–**c**) and mean ± s.d. (**d**–**f**). $^*P < 0.05$, $^{***}P < 0.001$, unpaired *t*-test (**a**–**e**), one-way ANOVA with Dunnett's test (**f**, **g**).

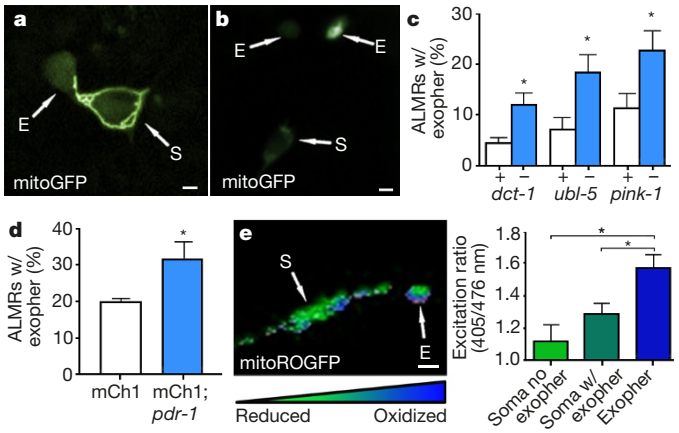

Figure 4 | Mitochondria can be extruded in exophers, and mitochondria with higher mitochondrial matrix oxidation might be preferentially extruded. a, Mitochondria in a budding exopher. Mitochondria form a ring around the somatic periphery, typical of young adulthood, with some mitochondria segregated into a putative exopher. Strain is *bzIs167*, green channel $P_{mec\text{-}4}$mitoGFP visualized. **b**, Mitochondrially localized mitoGFP (strain *bzIs167*) can be extruded in exophers; left exopher does not include substantial mitochondrial content, whereas the right exopher does. 10 out of 20 exophers scored with this reporter contained mitochondria. **c**, RNAi knockdown (blue) of mitochondrial health and function genes *ubl-5* (ref. 17), *pink-1*, and *dct-1* (ref. 15) increases the occurrence of exophers. White, empty vector control. *ubl-5* (3 trials), *pink-1* (4 trials), *dct-1* (3 trials). $n > 80$ total per condition. **d**, Genetic disruption of mitochondrial health and function increases the occurrence of exophers. Exopher levels were compared in the Is[$P_{mec\text{-}4}$mCh1]; *pdr-1(gk448)* mutant (mCh1; *pdr-1*), a Parkin homologue[16]; $n = 30$ per trial, 6 trials. **e**, Mitochondria segregated into exophers have higher relative oxidation levels than somatic mitochondria, as reported by mitoROGFP. Left, a pseudo-coloured image indicating relative emission levels at excitation wavelengths of 405/476 nm (blue, oxidized; green, reduced). Right, redox excitation ratio in exophers versus somas. $n = 10$ pairs of exophers with mitochondria and originating somas, strain is *zhsEx17* [$P_{mec\text{-}4}$mitoLS::ROGFP]. Of note, the soma shown exhibits locally concentrated oxidized mitochondria, indicating that oxidizing conditions are not restricted to exopher. Wild-type unstressed soma mitochondria have a typical 405/476 nm ratio of 1 (ref. 19); cells that form an exopher may experience increased levels of oxidation in the soma overall. All animals, adult day 2. Scale bars, 2 μm. Data are mean ± s.e.m. $^*P < 0.05$, unpaired *t*-test (**c, d**), one-way ANOVA with Tukey's test (**e**).

Second, the relative functionality of proteotoxically stressed neurons that have generated exophers is increased compared with neurons that did not extrude exophers. In blinded studies of a line expressing cyan fluorescent protein (CFP)-tagged Q128, which progressively impairs touch sensation[10], we found that midlife touch sensitivity is greater when ALMR had definitely produced an exopher at A2, as compared to age-matched siblings in which ALMR had not produced an exopher (Fig. 3e). Third, we identified *pod-1* and *emb-8* as polarity genes required in adults for exopher-genesis (Fig. 3f), and found that adult RNAi knockdown impaired midlife touch sensitivity (Fig. 3g). Although we cannot rule out that *pod-1* and *emb-8* RNAi interventions might generally disrupt adult neuronal function, taken together our data are consistent with a model in which adult neurons that do not make exophers become functionally compromised compared to those neurons that extruded offending contents. Overall, adult neurons seem to be healthier after a considerable expulsion of potentially toxic contents.

Considering the large apparent volume of exophers, we proposed that they might include organelles. Indeed, both lysosomes (Extended Data Fig. 4) and mitochondria (Fig. 4a, b, Extended Data Fig. 5) can be extruded in exophers. Mitochondrially localized GFP reporters revealed mitochondrial inclusion in budding and dissociated exophers, with punctate or filamentous morphology typical of adult mitochondrial networks (Fig. 4a, Extended Data Fig. 5a–c). To address whether impairing mitochondrial quality enhances the production of exophers, we genetically manipulated the mitophagy mediator *dct-1* (homologue of mammalian BNIP3), the human Parkinson's disease homologues *pink-1* (PINK)[15] and *pdr-1* (PARK2)[16] implicated in mitochondrial maintenance, and the mitochondrial unfolded protein response gene *ubl-5* (ref. 17) (Fig. 4c, d). We conclude that several genetic approaches that impair mitochondria can increase exopher-genesis.

To address the hypothesis that stressed or damaged mitochondria might be preferentially segregated to exophers, we used the mitochondrial reporter mitoROGFP, which changes its peak excitation wavelength from around 405 nm (oxidized) to 476 nm (reduced) according to the local oxidative environment[18,19]. We find a significant increase in the 405 nm (oxidized)/476 nm (reduced) excitation ratio of mitochondria in exophers compared to those in somas (Fig. 4e), roughly equivalent to the redox excitation ratio observed in *C. elegans* neurons subjected to H_2O_2-induced oxidative stress[19]. We confirmed higher oxidation scores using MitoTimer, an alternative reporter of

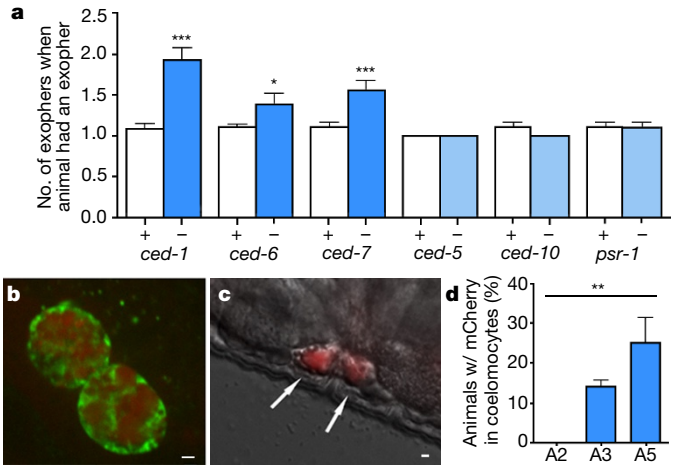

Figure 5 | Fluorescent mCherry escapes touch neurons and surrounding hypodermis to later concentrate in distant coelomocytes. a, *ced-1*, *ced-6* and *ced-7* mutations increase the number of ALMR neurons with two or more exophers, whereas *ced-5*, *ced-10* and *psr-1* mutations, acting in a parallel phagocytosis pathway, do not. Strain is *zdIs5*[$P_{mec\text{-}4}$GFP]; adult day 2, $n > 90$ total per strain, 3 trials. $^{*}P < 0.05$, $^{***}P < 0.001$, unpaired *t*-test (replicating RNAi data in Extended Data Fig. 6a). *ced-1*, *ced-6* and *ced-7* mutations do not increase the percentage of ALMRs that produce exophers (data not shown), but increase the detection of multiple exophers, suggesting a deficit in persistence rather than in generation. **b**, In older animals, coelomocytes (green) can concentrate fluorescent proteins that were originally expressed in touch neurons (red). Strain is Is[$P_{mec\text{-}4}$mCh1]; *pwIs979*[$P_{cup\text{-}4}$GFP*vps-29*]; adult day 6. **c**, mCherry localization in coelomocytes (arrows) can also be visualized with differential interference contrast (DIC) underlay for fluorescent image. Strain is Is[$P_{mec\text{-}4}$mCh1]; adult day 6. **d**, The number of coelomocytes containing mCherry released from touch neurons increased significantly over time. Is[$P_{mec\text{-}4}$mCh1] animals with an exopher on adult day 2 were segregated and scored for red fluorescence in coelomocytes on A2, A3 and A5; $n = 20$ per trial, 3 trials, $^{**}P < 0.01$, one-way ANOVA with Tukey's test. Scale bars, 2 μm. Data are mean ± s.e.m.

mitochondrial matrix oxidation[20] (Extended Data Fig. 5d). In addition, touch neurons of juglone-treated[21] *bzIs166*[$P_{mec\text{-}4}$mCherry]; *zhsEx17* [$P_{mec\text{-}4}$mitoLS::ROGFP] animals had significantly higher numbers of mitochondria-including exophers than matched controls (Extended Data Fig. 5e). Although compromised mitochondrial health may impair neuronal proteostasis, thus increasing exopher production, our data establish that touch neurons can eject mitochondria via exophers, which raises the intriguing possibility that exopher-genesis may constitute a previously unappreciated removal-based mechanism of mitochondrial homeostasis.

We next sought to determine the fate of the extruded exopher and its contents. With time, exopher fluorescence intensity diminishes or disappears (persistence times 1–12 h), possibly as exopher contents are degraded internally or digested by the neighbouring hypodermis that fully surrounds the touch neuron and has degradative capabilities. Disruption of the *C. elegans* apoptotic engulfment genes *ced-1* (homologue of mammalian CD91, LRP1 and MEGF10, and fly Draper), *ced-6* (GULP) and *ced-7* (ABC1) increases the detection of ALMR neurons that have extruded several exophers (Fig. 5a, Extended Data Fig. 6a); however, the genetic manipulation of a parallel engulfment pathway comprising *ced-2* (Crk-II), *ced-5* (DOCK180), *ced-10* (RAC1), *ced-12* (ELMO) and *psr-1* (PSR) did not change the frequency of exopher generation or the detection of multiple exophers. Moreover, we did not detect the apoptotic 'eat-me' signal phosphatidylserine on the exopher surface using a widely expressed phosphatidylserine-binding annexin-V::GFP (0 out of 43 exophers; Extended Data Fig. 6b). Our data suggest that hypodermal recognition/degradation of exophers and their contents occurs by mechanisms that are at least in part distinct from the classical removal of apoptotic corpses, but involve the CED-1, CED-6 and CED-7 proteins. Electron microscopy studies also show that the hypodermis may mediate the degradation of at least some exopher contents (Extended Data Fig. 2d–f, h).

The lack of a detectable phosphatidylserine signal on exophers raised the question as to whether at least some exopher contents might be destined to elude hypodermal degradation. Indeed, fluorescent mCherry protein that was originally expressed specifically in touch neurons, or fluorescent DiI loaded into dye-filling neurons, appeared later in distant scavenger coelomocytes (Fig. 5b–d, Extended Data Fig. 6c). Blocking coelomocyte uptake capacity by *cup-4* mutation[22] caused fluorescent particles to accumulate outside neurons, possibly within the pseudocoelom (body cavity; Extended Data Fig. 6d, e). We conclude that some exopher contents transit the hypodermal tissue to be released into the pseudocoelomic fluid, from which materials can later be taken up by distant coelomocytes. Exophers can therefore mediate transfer of neuronal materials to remote cells.

Considerable excitement in the neurodegenerative disease field has been generated by the findings that mammalian neurons can extrude conformational disease proteins, including in Alzheimer's, Parkinson's and prion disease[23]. The production of exophers in *C. elegans* constitutes a newly identified mechanism by which neurons can transfer cellular material (preferentially neurotoxic species) to other cells. Notably, in a *C. elegans* muscle model of prion toxicity, offending prion proteins were transferred among muscle cells and ultimately localized to coelomocytes[24]. We speculate that the basic mechanism we document here may correspond to a conserved pathway for the transfer of toxic contents out of many cell types. In this regard, it may be noteworthy that mammalian aggregated poly-Q-expanded huntingtin can transfer between neurons via tunnelling nanotubes[25–27] that resemble thin connections between *C. elegans* somas and exophers, and that neuronal polyQ in *Drosophila* is transferred to glia via a process that requires the CED-1 homologue, Draper[28].

Recent reports show that mitochondria can transfer out of specific cells to contribute positive roles (mesenchymal stem cells via tunnelling nanotubes[29]; astrocytes to neurons in a stroke model[30]), but our study underscores a generally underappreciated option for mitochondrial quality control: mitochondrial expulsion. The mitochondrial expulsion we report in *C. elegans* touch neurons has a notable mammalian counterpart: mouse mitochondria originating in retinal ganglion cells can be extruded into neighbouring astrocytes for degradation[6] (with some similar morphology to *C. elegans* exophers; see fig. 1e of ref. 6). Although further study will be required to establish definitively the health status and fates of transferred mitochondria in the *C. elegans* model, it is tempting to speculate that transcellular degradation of mitochondria may be a more broadly used mechanism of mitochondrial quality control than currently appreciated, with associated potential importance in neuronal health.

Overall, although further experiments are needed to determine the detailed mechanisms at play and validate the proposed functions of exophers in proteostasis and the removal of damaged organelles, we suggest that exopher production is a previously unrecognized mechanism for clearing out accumulating protein aggregates and dysfunctional organelles that threaten neuronal homeostasis (Extended Data Fig. 7). The analogous process in mammals could enable the transfer of misfolded protein and/or dysfunctional mitochondria to neighbouring cells, promoting human pathology in neurodegenerative disease if compromised. Mechanistic dissection of this new aspect of proteostasis and mitochondrial homeostasis should thus inform on fundamental mechanisms of neuronal maintenance and suggest targets for intervention in neurodegenerative disease.

Online Content Methods, along with any additional Extended Data display items and Source Data, are available in the online version of the paper; references unique to these sections appear only in the online paper.

Received 21 July 2015; accepted 3 January 2017.
Published online 8 February 2017.

1. Yankner, B. A., Lu, T. & Loerch, P. The aging brain. *Annu. Rev. Pathol.* **3,** 41–66 (2008).
2. Federico, A. *et al.* Mitochondria, oxidative stress and neurodegeneration. *J. Neurol. Sci.* **322,** 254–262 (2012).
3. Morimoto, R. I. Proteotoxic stress and inducible chaperone networks in neurodegenerative disease and aging. *Genes Dev.* **22,** 1427–1438 (2008).
4. Ben-Gedalya, T. & Cohen, E. Quality control compartments coming of age. *Traffic* **13,** 635–642 (2012).
5. Lee, S. J., Desplats, P., Sigurdson, C., Tsigelny, I. & Masliah, E. Cell-to-cell transmission of non-prion protein aggregates. *Nat. Rev. Neurol.* **6,** 702–706 (2010).
6. Davis, C. H. *et al.* Transcellular degradation of axonal mitochondria. *Proc. Natl Acad. Sci. USA* **111,** 9633–9638 (2014).
7. Toth, M. L. *et al.* Neurite sprouting and synapse deterioration in the aging *Caenorhabditis elegans* nervous system. *J. Neurosci.* **32,** 8778–8790 (2012).
8. Craig, A. L., Moser, S. C., Bailly, A. P. & Gartner, A. Methods for studying the DNA damage response in the *Caenorhabdatis elegans* germ line. *Methods Cell Biol.* **107,** 321–352 (2012).
9. Perkins, L. A., Hedgecock, E. M., Thomson, J. N. & Culotti, J. G. Mutant sensory cilia in the nematode *Caenorhabditis elegans*. *Dev. Biol.* **117,** 456–487 (1986).
10. Parker, J. A. *et al.* Expanded polyglutamines in *Caenorhabditis elegans* cause axonal abnormalities and severe dysfunction of PLM mechanosensory neurons without cell death. *Proc. Natl Acad. Sci. USA* **98,** 13318–13323 (2001).
11. Vayndorf, E. M. *et al.* Morphological remodeling of *C. elegans* neurons during aging is modified by compromised protein homeostasis. *NPJ Aging Mech. Dis.* **2,** 16001 (2016).
12. Labbadia, J. & Morimoto, R. I. Proteostasis and longevity: when does aging really begin? *F1000Prime Rep.* **6,** 7 (2014).
13. Labbadia, J. & Morimoto, R. I. Repression of the heat shock response is a programmed event at the onset of reproduction. *Mol. Cell* **59,** 639–650 (2015).
14. Liu, G., Rogers, J., Murphy, C. T. & Rongo, C. EGF signalling activates the ubiquitin proteasome system to modulate *C. elegans* lifespan. *EMBO J.* **30,** 2990–3003 (2011).
15. Sämann, J. *et al. Caenorhabditits elegans* LRK-1 and PINK-1 act antagonistically in stress response and neurite outgrowth. *J. Biol. Chem.* **284,** 16482–16491 (2009).
16. Springer, W., Hoppe, T., Schmidt, E. & Baumeister, R. A *Caenorhabditis elegans* Parkin mutant with altered solubility couples alpha-synuclein aggregation to proteotoxic stress. *Hum. Mol. Genet.* **14,** 3407–3423 (2005).
17. Benedetti, C., Haynes, C. M., Yang, Y., Harding, H. P. & Ron, D. Ubiquitin-like protein 5 positively regulates chaperone gene expression in the mitochondrial unfolded protein response. *Genetics* **174,** 229–239 (2006).
18. Cannon, M. B. & Remington, S. J. Redox-sensitive green fluorescent protein: probes for dynamic intracellular redox responses. A review. *Methods Mol. Biol.* **476,** 50–64 (2008).
19. Ghose, P., Park, E. C., Tabakin, A., Salazar-Vasquez, N. & Rongo, C. Anoxia-reoxygenation regulates mitochondrial dynamics through the hypoxia response pathway, SKN-1/Nrf, and stomatin-like protein STL-1/SLP-2. *PLoS Genet.* **9,** e1004063 (2013).
20. Laker, R. C. *et al.* A novel MitoTimer reporter gene for mitochondrial content, structure, stress, and damage *in vivo*. *J. Biol. Chem.* **289,** 12005–12015 (2014).
21. Ji, Y. B., Qu, Z. Y. & Zou, X. Juglone-induced apoptosis in human gastric cancer SGC-7901 cells via the mitochondrial pathway. *Exp. Toxicol. Pathol.* **63,** 69–78 (2011).
22. Patton, A. *et al.* Endocytosis function of a ligand-gated ion channel homolog in *Caenorhabditis elegans*. *Curr. Biol.* **15,** 1045–1050 (2005).
23. Nath, S. *et al.* Spreading of neurodegenerative pathology via neuron-to-neuron transmission of β-amyloid. *J. Neurosci.* **32,** 8767–8777 (2012).
24. Nussbaum-Krammer, C. I., Park, K. W., Li, L., Melki, R. & Morimoto, R. I. Spreading of a prion domain from cell-to-cell by vesicular transport in *Caenorhabditis elegans*. *PLoS Genet.* **9,** e1003351 (2013).
25. Costanzo, M. *et al.* Transfer of polyglutamine aggregates in neuronal cells occurs in tunneling nanotubes. *J. Cell Sci.* **126,** 3678–3685 (2013).
26. Abounit, S. & Zurzolo, C. Wiring through tunneling nanotubes—from electrical signals to organelle transfer. *J. Cell Sci.* **125,** 1089–1098 (2012).
27. Gousset, K. *et al.* Prions hijack tunnelling nanotubes for intercellular spread. *Nat. Cell Biol.* **11,** 328–336 (2009).
28. Pearce, M. M., Spartz, E. J., Hong, W., Luo, L. & Kopito, R. R. Prion-like transmission of neuronal huntingtin aggregates to phagocytic glia in the *Drosophila* brain. *Nat. Commun.* **6,** 6768 (2015).
29. Pasquier, J. *et al.* Preferential transfer of mitochondria from endothelial to cancer cells through tunneling nanotubes modulates chemoresistance. *J. Transl. Med.* **11,** 94 (2013).
30. Hayakawa, K. *et al.* Transfer of mitochondria from astrocytes to neurons after stroke. *Nature* **535,** 551–555 (2016).

Supplementary Information is available in the online version of the paper.

Acknowledgements We thank B. Grant for expert advice, C. Reina for time-lapse microscopy help; N. Kane and J. Kramer for confocal microscopy assistance; and H. Ushakov for construction of some genetic lines. We thank G. Perumal and F. Macaluso for help with HPF fixations, and C. Crocker for the cartoon in Extended Data Fig. 2b. F. Sesti and M. Hilliard supplied *C. elegans* strains; A. Mendenhall, B. Sands and R. Brent constructed the MOSCI mitoTimer strain. Research was supported by the National Institutes of Health under award numbers 1R01NS086064 and 1R01AG046358. I.M. and R.J.G. were supported by the National Institute of General Medical Sciences under award number T32 GM008339. K.C.N. and D.H.H. were supported by NIH OD10943 (to D.H.H.); Core EM facilities (D.H.H.) NICHD P30 HD71593 for the RFK-IDDRC at Albert Einstein College of Medicine. Some strains were provided by the CGC, which is funded by NIH Office of Research Infrastructure Programs (P40 OD010440). Content is solely the responsibility of the authors and does not necessarily represent the official views of the National Institutes of Health.

Author Contributions I.M., M.L.T., M.L.A., R.J.G. and G.H. conducted and designed experiments along with M.D. I.M. and M.D. wrote the manuscript with input from R.J.G., M.L.A. and M.L.T. C.V.G. and D.T. carried out calcium connection experiments. K.C.N. and D.H.H. carried out electron microscopy. J.A.P. and C.N. supplied the Q128 reagent and manuscript critiques.

Author Information Reprints and permissions information is available at www.nature.com/reprints. The authors declare no competing financial interests. Readers are welcome to comment on the online version of the paper. Correspondence and requests for materials should be addressed to M.D. (driscoll@dls.rutgers.edu).

Reviewer Information *Nature* thanks C. Bargmann, D. Divizio and the other anonymous reviewer(s) for their contribution to the peer review of this work.

METHODS

Strains and media. *C. elegans* strains were cultured at 20 °C with standard methods[31]. Strains used were SK4005 *zdIs5*[P_{mec-4}GFP] (abbreviated in the text as Is[P_{mec-4}GFP], ZB4065 *bzIs166*[P_{mec-4}mCherry1] (abbreviated in the text as Is[P_{mec-4}mCh1]), ZB4066 *bzIs167*[P_{mec-4}mitoGFP P_{mec-4}mCherry2] (abbreviated in the text as Is[P_{mec-4}mCh2]), ZB4067 *bzIs167*[P_{mec-4}mitoGFP P_{mec-4}mCherry2]; *igIs1*[P_{mec-7}YFP P_{mec-3}htt57Q128::cfp *lin-15*$^{+}$][10] (abbreviated in the text as Is[mCh2; Q128CFP]), *sesIs2512*[P_{gcy-5}GFP], *sesIs25*[$P_{flp-6}A\beta_{1-42}$; P_{gcy-5}GFP][32], KWN176 *rnyIs014*[P_{mec-4}mCherry *unc-119(+)*], ZB4071 *bzIs169*[P_{mec-18}*sid-1* P_{sng-1}YFP]; *bzIs101*[P_{mec-4}mCherry; $P_{unc-119}$$^{+}$], ZB4087 *bzIs169*[$P_{mec-18}$*sid-1*$P_{sng-1}$ YFP]; *bzIs101*[P_{mec-4}mCherry; $P_{unc-119}$$^{+}$]; *hsf-1(sy441)*, BZ555 *egIs1*[P_{dat-1}GFP], ZB4070 *bzIs168*[P_{mec-7}LMP-1::GFP], ZB4509 *bzIs166*[P_{mec-4}mCherry]; *bzIs168* [P_{mec-7}LMP-1::GFP], ZB4082 *cup-4(ok837); bzIs166*[P_{mec-4}mCherry], ZB4083 *smIS76* [P_{hsp-16}ANV::GFP][33]; *bzIs166*[P_{mec-4}mCherry], ZB4084 *hsf-1(sy441); zdIs5*[P_{mec-4}GFP], ZB4085 *hsf-1(sy441); bzIs166*[P_{mec-4}mCherry], ZB4086 *zdIs5*[P_{mec-4}GFP]; *bzIs166*[P_{mec-4}mCherry], PTN73 *pha-1(e2123); him-5(e1490); zhsEx17*[P_{mec-4}mitoLS::ROGFP], RBW2834 rbw2834Si[P_{mec-3}mitoTimer::T54, Cb-*unc-119* + II ttTi5605] in *unc-119(ed3)*[20], QH3738 *ced-1(e1735); zdIs5*, QH3737*ced-6(n1813)*; *zdIs5*, QH4623 *ced-5(n1812); zdIs5*, QH3768 *ced-7(n2690)*; *zdIs5*, QH3130 *ced-10(n3246); zdIs5*, QH3533 *psr-1(ok714); zdIs5* (ref. 34), ZB4526 *bzIs166*[P_{mec-4}mCherry]; *pdr-1(gk448)*, ZB4525 *bzIs166*[P_{mec-4}mCherry]; (*pwIs979* [P_{cup-4}GFP::*vps-29* Cb-unc-119], ZB4528 *bzIs166*[P_{mec-4}mCherry]; *zhsEx17* [P_{mec-4}mitoLS::ROGFP], ZB4059 *bzIs163*[P_{mec-4}GCaMP3.0::SL2::mCherry], ZB4524 *bzEx242*[P_{mec-4}PH(plcDelta)::GFP][35], and wild type N2.

RNAi was administered through feeding animals with RNAi-expressing bacteria with standard methods[36] with touch neuron RNAi-enhanced via *sid-1* expression[37]. Exophers are readily visible at 400× total magnification, with high-power dissecting microscopes. In general, exophers have the following features: a ∼4 μm membrane-bound vesicle extruded from a neuron via a mechanism that temporarily includes a thin filamentous connection to the originating soma, but eventually breaks off. Contents of exophers can include neurotoxic proteins, mitochondria, and lysosomes; exophers are produced by native amphid neurons as visualized after dye-filling.

Age synchronization and RNAi screening. To synchronize animals, L4-stage hermaphrodites were selected and moved to test plates. The day after moving was considered adult day 1, and animals were scored on adult day 2 for the occurrence of exophers. For scoring of exophers, animals were immobilized by adding 100 μl of 10 mM tetramisole to the surface of the plate. Animals were measured on the plate with a Kramer dissecting scope with a 20× objective. The ALMR neuron was scored for the presence of an exopher, which was counted if greater than one-quarter the size of the soma, as a threshold against inclusion of smaller species of extracellular vesicles. Exophers were also visible in live animals without anaesthetic. RNAi experiments had a negative empty vector control. An mCherry knockdown was used to confirm RNAi had an effect in the neurons of interest. RNAi screens were performed with the strain *bzIs169*[P_{mec-18}*sid-1* P_{sng-1}YFP]; *bzIs101*[P_{mec-4}mCherry; *unc-119*$^{+}$]. All genes were independently screened a minimum of three times.

Microscopy techniques. For imaging, animals were mounted by placing them in a drop of cold, liquid 36% Pluronic F-127 with 1 mM tetramisole solution and pressed between two coverslips. The slides were brought to room temperature, solidifying the Pluronic F-127 gel and immobilizing the animals. Co-localization images were made using iVision software. Images were taken using a Zeiss Imager D1m upright compound microscope with a 40× dry objective. For confocal imaging, animals were immobilized by using 7.5% M9 agarose pads with 2.5 μl PolySciences 0.05 μm polystyrene microspheres. A Zeiss spinning disk confocal upright microscope with 100× oil immersion objective was used for select images to show additional details, including lysosomal imaging and connection imaging.

MitoROGFP imaging and quantification. Adult day 2 PTN73 *pha-1(e2123); him-5(e1490); zhsEx17*[P_{mec-4}mitoLS::ROGFP] animals were mounted as above on a Leica SP5 II confocal microscope (Leica Microsystems) with a 63× oil immersion lens. Samples were alternately excited with a 30% power 405 nm UV laser and a 30% power 476 nm visible laser with a sequential line scanning method. Emission was detected by HYD1 photon counting at 508–513 nm. Images were quantified using ImageJ. Images were thresholded to remove background. The 405 nm channel was divided by the 476 nm channel, and ROI measurement was used to quantify mean intensities.

MitoTimer imaging and quantification. MitoTimer encodes a dsRed derivative that fluoresces green when reduced (first synthesized), but irreversibly shifts to red fluorescence as it oxidizes[20]. Adult day 2 rbw2834Si[P_{mec-3}::mitotimer::T54, CB-*unc-119* + II ttTi5605] in *unc-119 (ed3)* animals were mounted as above on a Zeiss Imager D1m upright compound microscope with a 63× oil immersion lens. Samples were alternately measured under GFP and dsRed channels, keeping light intensity and exposure times constant between images. Images were quantified using ImageJ by selecting the ROI, subtracting the background, measuring red and green intensities, and calculating the red/green ratio.

Fluorescence quantification. Fluorescence quantification was performed in ImageJ by selecting the ROI, measuring the mean intensity, and subtracting background intensity.

Time-lapse imaging. Time-lapse imaging was performed with a 100× oil immersion objective with a motorized stage. 15 animals were mounted to a slide using 7.5% M9 agarose pads with 2.5 μl PolySciences 0.05 μm polystyrene microspheres; the coverslip was sealed with a 60:40 mix of Vaseline and paraffin wax. An iVision script was used to image selected locations every 8–15 min for 12 h. Image analysis and video compilation were done manually.

Dye-filling. We dye-filled the amphid neurons, which are open to the environment[9]. Animals were washed off a plate into a 1.5 ml centrifuge tube with 1 ml M9 and 10 μl of 1 mM DiI. Animals were allowed to soak at room temperature for 3 h. Animals were washed with M9 twice before mounting onto slides for imaging.

Longitudinal measurements. 50 animals were synchronized at the L4 stage and 25 animals were measured on subsequent adult days, directly from the plate without anesthetics using a Kramer dissecting microscope. The animals were transferred to fresh plates every 2 days until adult day 8 to prevent crowding and starvation.

DAPI staining. DAPI staining was performed after wash-harvesting with PBS and permeabilizing the membrane in a −80 °C freezer for 10 min. After thawing, the supernatant was removed and animals were re-suspended in 1 ml cold methanol and incubated 5 min for fixation. Animals were washed with PBS twice and then stained in a 1 ml DAPI solution (200 ng ml^{-1} in PBS) for 30 min before mounting for microscopy.

Size measurement. Exopher and cell size was performed by measuring pixel length with Photoshop and comparing to a calibration scale for each objective used. Width was measured at the widest point.

Drug assays. MG132 (Sigma-Aldrich C2211) and spautin-1 (ref. 38) (Sigma-Aldrich SML0440) were dissolved in DMSO at 10 mM and 1 mM, respectively, and administered by placing 30 μl of the solution over the bacterial food lawn.

Juglone exposure leads to an increase in intracellular reactive oxygen species production, most notably superoxide radicals, and can cause mitochondrial membrane depolarization and opening of permeability transition pores, allowing pro-apoptotic cytochrome C to escape from the mitochondria[21]. Juglone (Sigma-Aldrich 59990) was dissolved to a final concentration of 230 μM in a solution of 0.23% (v/v) ethanol in M9. Adult day 1 worms were transferred into either a 1 ml tube of the juglone solution or a 1 ml control tube of 0.23% (v/v) ethanol in M9 for 90 min. Animals were washed with M9 buffer, centrifuged, and recovered onto a microscope slide for imaging.

Hydroxyurea (Sigma-Aldrich H8627) was dissolved in distilled water to make a 1 M solution, of which 250 ml was added to a standard seeded NGM plate to reach a working concentration of 25 mM[8]. Plate was left at room temperature for 6 h to allow for complete diffusion before transferring adult day 1 animals for measurement 24 h later on adult day 2.

Touch-sensitivity assay. To assay for touch sensitivity, animals were stroked with a calibrated force probe on the anterior and posterior halves of the body. Reversal was an indication of a positive response. Animals responding to at least 3 out of 5 touches were considered sensitive. Animals responding to 2 or fewer touches were considered not sensitive.

Aggregate measurements. Q128 aggregates can be visually distinguished in touch neuron somas with a 20× objective[11,39]. The aggregate exopher prediction experiment was done by separating day 1 adult animals into two populations, those that had one visible aggregate in the ALMR neuron and those that had two or more. The two populations were scored on the next day for exophers extruded from the ALMR neuron.

Electron microscopy. Young adults were screened by light microscopy to identify samples in which the ALM neurons had recently expelled an exopher. These animals were prepared for transmission electron microscopy (TEM) analysis approximately 3 h after initial selection by high pressure freezing and freeze substitution (HPF/FS) following a standard protocol for preservation of ultrastructure[40]. In brief, after HPF, animals were exposed to 1% osmium tetroxide in acetone with 2% water added, kept at −90 °C for 5–6 days before slowly warming back to room temperature. Samples were rinsed in cold acetone and embedded in plastic resin before curing at high temperature for 1–2 days. Serial thin sections were collected on plastic-coated slot grids, post-stained with uranyl acetate, and examined with a Philips CM10 electron microscope. By looking in transverse sections for landmarks such as the second bulb of the pharynx, it was possible to reach the vicinity of the ALM soma before collecting about 1,500 serial thin transverse sections. Having found the soma, one could then explore the region 30–50 μm posterior to the ALMR for evidence of the exopher.

FRAP analysis. Synchronized Is[$P_{mec\text{-}4}$mCh1] adult day 2 animals were immobilized on 7.5% M9 agarose pads with 2.5 µl PolySciences 0.05 µm polystyrene microspheres. Exopher centres were photo-bleached with 7 pulses of the MicroPoint pulsed nitrogen pumped dye laser (neutral density filter at position 9, Lumencor solid state light source) attached to a Zeiss Inverted Axio Observer microscope (100× 1.4 numerical aperture (NA) objective) on an anti-vibration table. 1 frame was recorded every 5 s using constant excitation intensity and exposure time with a Qimaging EXi Blue camera. Images were analysed with ImageJ. Exopher fluorescence intensity was normalized to the intensity of the first data point in each series.

GCaMP studies on axotomized neurons with connected exophers. Adult day 4 *bzIs163*[$P_{mec\text{-}4}$GCaMP3.0::SL2::mCherry] worms expressing the genetically encoded calcium indicator GCaMP3.0 in the mechanosensory neurons were immobilized with 0.1% tetramisole on 3% agar pads. As described previously[41], a Ti:Sapphire laser system was used to perform axotomy (10 KHz pulse rate, 15 nJ per pulse). Axons were cut 20 µm from the soma with five rapid exposures (0.25 s) to the laser beam, resulting in vaporization of the axon at the target point. Time-lapse images were taken 20 s before cutting and up to 1 min after the cut, 1 frame s^{-1}. Two individuals with exophers connected to the soma and three individuals with exophers not connected to the soma were analysed, with only the connected exophers showing any calcium response to axotomy.

Blinding. Blinding was performed by laboratory members uninvolved in the relevant experiment. Strain and treatment information were recorded in a secret key and replaced with a symbol on the measurement plates. The data were unblinded following completion of the experiment. Animals were allocated to measurement plates randomly.

Statistical analysis. Sample size was established using G-power software to be able to detect moderate effects with 80% power at $P = 0.05$ after a replicate for routine measurements. For higher throughput, larger screens were designed to have an 80% power to meet the re-screening cutoff of $P = 0.25$. Data were considered normal by the Shapiro–Wilk normality test.

Because of variable RNAi outcomes in different trials, exopher numbers were always compared to the empty vector control for that particular experiment. Statistics were performed using a two tailed unpaired *t*-test between the trial means, considering neurons with an exopher as 1 and neurons without an exopher as 0. One-way ANOVA was performed with Dunnett's test when multiple samples were compared to a single control, and with Tukey's test when multiple samples were compared to each other. Details of statistics are described in figure legends.

Data availability. The data that support the findings of this study are available from the corresponding author upon reasonable request.

31. Brenner, S. The genetics of *Caenorhabditis elegans*. *Genetics* **77,** 71–94 (1974).
32. Duan, Z. & Sesti, F. A *Caenorhabditis elegans* model system for amylopathy study. *J. Vis. Exp.* **75,** 50435 (2013).
33. Mapes, J. *et al.* CED-1, CED-7, and TTR-52 regulate surface phosphatidylserine expression on apoptotic and phagocytic cells. *Curr. Biol.* **22,** 1267–1275 (2012).
34. Neumann, B. *et al.* EFF-1-mediated regenerative axonal fusion requires components of the apoptotic pathway. *Nature* **517,** 219–222 (2015).
35. Kachur, T. M., Audhya, A. & Pilgrim, D. B. UNC-45 is required for NMY-2 contractile function in early embryonic polarity establishment and germline cellularization in *C. elegans*. *Dev. Biol.* **314,** 287–299 (2008).
36. Kamath, R. S. & Ahringer, J. Genome-wide RNAi screening in *Caenorhabditis elegans*. *Methods* **30,** 313–321 (2003).
37. Calixto, A., Chelur, D., Topalidou, I., Chen, X. & Chalfie, M. Enhanced neuronal RNAi in *C. elegans* using SID-1. *Nat. Methods* **7,** 554–559 (2010).
38. Liu, J. *et al.* Beclin1 controls the levels of p53 by regulating the deubiquitination activity of USP10 and USP13. *Cell* **147,** 223–234 (2011).
39. Scerbak, C. *et al.* Insulin signaling in the aging of healthy and proteotoxically stressed mechanosensory neurons. *Front. Genet.* **5,** 212 (2014).
40. Topalidou, I. *et al.* Genetically separable functions of the MEC-17 tubulin acetyltransferase affect microtubule organization. *Curr. Biol.* **22,** 1057–1065 (2012).
41. Gabel, C. V., Antoine, F., Chuang, C. F., Samuel, A. D. & Chang, C. Distinct cellular and molecular mechanisms mediate initial axon development and adult-stage axon regeneration in *C. elegans*. *Development* **135,** 1129–1136 (2008).
42. Kopito, R. R. Aggresomes, inclusion bodies and protein aggregation. *Trends Cell Biol.* **10,** 524–530 (2000).
43. Hermann, G. J. *et al.* Genetic analysis of lysosomal trafficking in *Caenorhabditis elegans*. *Mol. Biol. Cell* **16,** 3273–3288 (2005).
44. Zhou, Z., Hartwieg, E. & Horvitz, H. R. CED-1 is a transmembrane receptor that mediates cell corpse engulfment in *C. elegans*. *Cell* **104,** 43–56 (2001).
45. Hong, Y., Roy, R. & Ambros, V. Developmental regulation of a cyclin-dependent kinase inhibitor controls postembryonic cell cycle progression in *Caenorhabditis elegans*. *Development* **125,** 3585–3597 (1998).
46. Kastelowitz, N. & Yin, H. Exosomes and microvesicles: identification and targeting by particle size and lipid chemical probes. *ChemBioChem.* **15,** 923–928 (2014).
47. Cocucci, E. & Meldolesi, J. Ectosomes and exosomes: shedding the confusion between extracellular vesicles. *Trends Cell Biol.* **25,** 364–372 (2015).
48. Thery, C., Zitvogel, L. & Amigorena, S. Exosomes: composition, biogenesis and function. *Nat. Rev. Immunol.* **2,** 569–579 (2002).
49. Ma, L. *et al.* Discovery of the migrasome, an organelle mediating release of cytoplasmic contents during cell migration. *Cell Res.* **25,** 24–38 (2015).

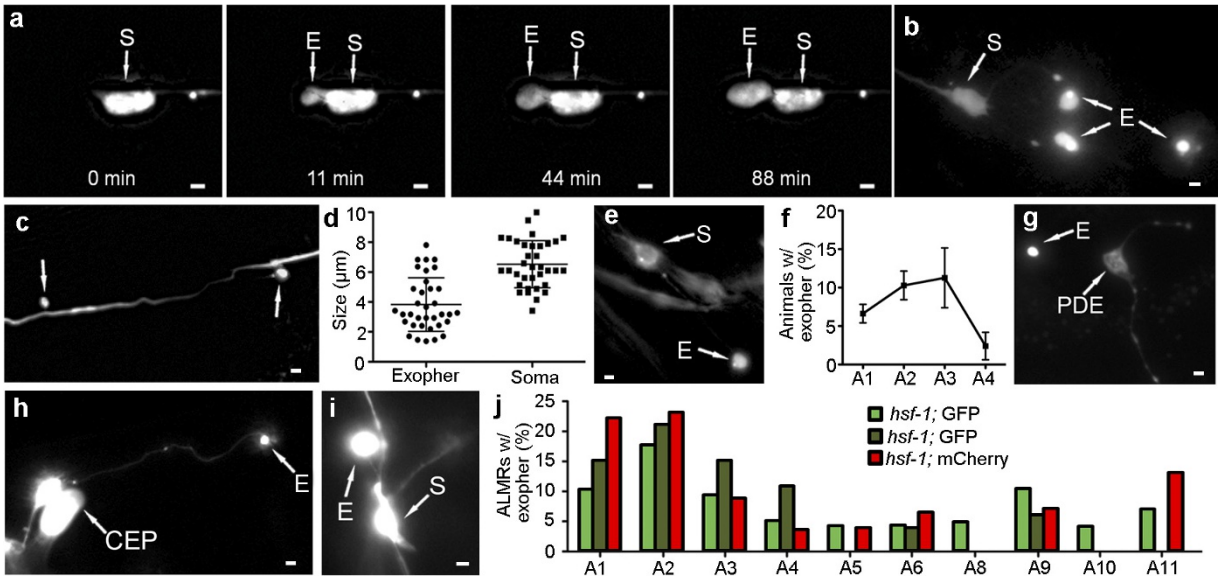

Extended Data Figure 1 | Morphological features of exophers derived from touch neurons. a, An exopher is generated with evident filling and growth. The exopher size increased for more than 1 h, specifically in the exopher compartment, possibly via continual delivery of materials to the exopher after initial formation (see Supplementary Video 2). Strain is Is[$P_{mec\text{-}4}$mCh1], adult day 2. **b**, An ALMR soma with multiple exophers. Strain is Is[$P_{mec\text{-}4}$mCh2], adult day 2. **c**, A rare instance of an ALM neuron with exophers that appear extruded from the dendrite (arrows). Strain is Is[$P_{mec\text{-}4}$mCh1], adult day 2. **d**, Size measurements for somas (squares) and exophers (circles). Data are combined for exophers scored in different backgrounds, $n = 35$. Values analysed in Extended Data Table 2. **e**, Example of a exopher derived from a dye-filled amphid neuron. We identified exophers from dye-filled amphids, some of which appeared attached. Neuronal exophers are thus not induced solely in response to expression of foreign proteins, but can be produced from neurons that express only native proteins. See Extended Data Fig. 6c for a second example of a dye-filled exopher. **f**, Early adult longitudinal time-course on DiI-soaked wild-type N2. Dye-filled chemosensory amphid neurons also produce exophers with a peak early in life in wild-type animals. The production of exophers in this study reflects the extrusion of native neuronal contents, as no fluorescent transgene is introduced. Total $n > 150$, 3 trials. **g**, **h**, Dopaminergic PDE and CEP neurons can produce exophers. **g**, GFP-expressing PDE neuron with an anterior exopher indicated (8 out of 450 had exophers, typical of the low rate observed with GFP reporters in touch neurons). **h**, CEP neuron with an associated exopher. Strain is *egIs1*[$P_{dat\text{-}1}$GFP]; adult day 2. **i**, ASER neurons can form exophers. Strain is *sesIs25*[$P_{flp\text{-}6}$Aβ; $P_{gcy\text{-}5}$GFP][32]; adult day 2. **j**, The onset of touch neuron exophers in an *hsf-1* mutant background occurs 1 day earlier than wild-type touch neurons, beginning on adult day 1, but follows the general trend of high incidence early in adult life. Longitudinal study with Is[$P_{mec\text{-}4}$GFP]; *hsf-1(sy441)* (2 green trials, starting $n = 25$), and Is[$P_{mec\text{-}4}$mCh1]; *hsf-1(sy441)* (red, starting $n = 25$). We observed a similar temporal pattern for Is[$P_{mec\text{-}4}$mCh2]; [$P_{mec\text{-}3}$Q128CFP] (data not shown). A late onset peak might not be apparent owing to sickness of *hsf-1* mutants later in life. Data in **d** and **f** are mean ± s.e.m. Data in **j** are from single longitudinal trials and thus error bars are not included. Scale bars, 2 µm.

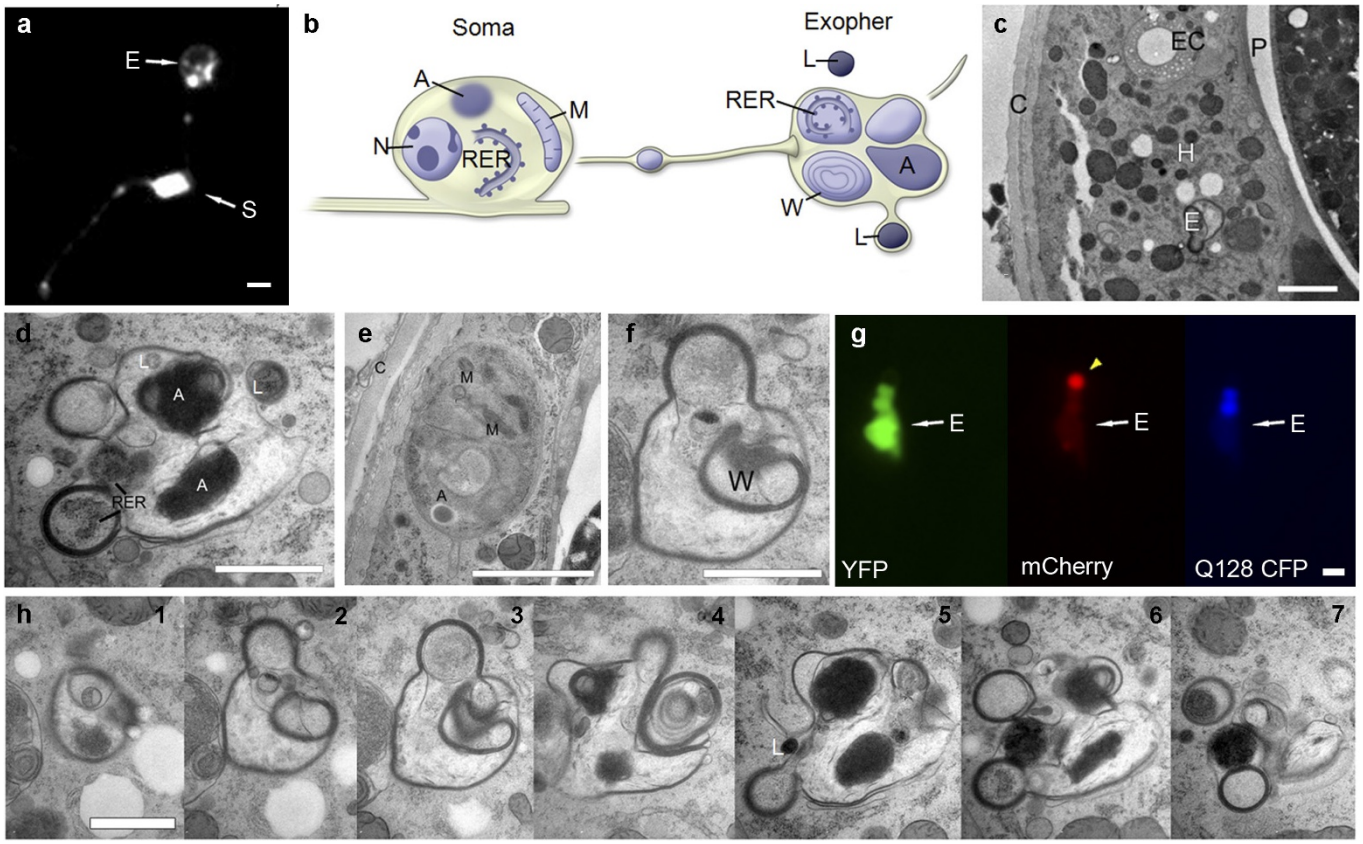

Extended Data Figure 2 | Electron microscopy images of an extruded exopher. a, A membrane GFP reporter in a PVM neuron reveals that exophers contain membrane. Strain is $P_{mec\text{-}4}$PH(plcDelta)::GFP (ref. 35). **b**, Relationship of exopher to ALMR soma. Schematic view from a lateral aspect (anterior to the left). ALMR soma remains connected to its primary dendrite. Several smaller membrane-bound tubes extend away from the soma, containing small expelled items, such as the large vesicle shown. The ALMR nucleus (N) is intact, but pushed to an eccentric position by cytoplasmic inclusions. The soma contains intact rough endoplasmic reticulum (RER), mitochondria (M), small vesicles (not shown), and larger protein aggregates (A). The exopher comprises heterogeneous contents. Exopher exterior is completely bounded by hypodermal plasma membrane, so exopher contents are not in immediate contact with hypodermal cytoplasm. A double membrane is often observed where the exopher is likely to supply the inner bilayer, and the hypodermis contributes the outer bilayer. Additional, separate membrane-bound items lie peripherally (not shown; but see **h**), which may be breakdown products from an earlier, larger stage of the exopher. Most internal exopher contents have their own membrane boundaries, but diffuse material (not shown; but see **c**, **e**) fills spaces around those membrane-bound objects. Membrane-bound contents include portions of neuronal cytoplasm holding intact RER, large protein aggregates, and complex whorls of membrane (W) that seem to enclose empty space. Two lysosomes (L) are shown, one in the process of fusing to exopher outer membrane. A tube is shown extending (far right) towards the pseudocoelom, which might offer a route for elimination of contents that cannot be degraded during hypodermal transit. Cartoon designed by and published with permission of C. Crocker. **c**, **d**, **f**, **h**, TEM views of an exopher, emitted from cell body in **e**. **c**, The exopher is fully embedded within hypodermis (H), seen from anterior aspect (thus left/right reversed). Strain is Is[$P_{mec\text{-}4}$ mCh1]; Is[$P_{mec\text{-}4}$GFP]. C, animal cuticle. Exopher is 1.5 μm, similar in size to the excretory canal (EC), and lies closer to the pseudocoelom (P), whereas the ALMR neuron soma lies closer to cuticle (see **e**). Jagged white spaces running vertically through hypodermis are an artefact where tissue cracked during processing. **d**, The exopher is characterized by many small round protrusions and involuted portions, with multiple membrane layers. The main exopher complex has a complete plasma membrane surrounding it. **e**, The originating ALMR neuron still has intact cell and nuclear membranes. Aggregate within soma is not membrane bound, resembling a mammalian aggresome[42]. Electron density of the neuronal cytoplasm is darker than that of surrounding hypodermis, and mitochondria of hypodermis are far larger than those of the neuron. **f**, The exopher is surrounded by a continuous membrane and contains electron-lucent materials and electron-dense membrane whorls. **g**, Fluorescent microscopy of exopher in a day 2 animal, expressing soluble YFP, CFP-tagged Q128 fusion, and aggregation-prone mCherry. mCherry has a bright spot that excludes the other two signals (arrowhead). Q128–CFP and YFP are localized in the middle and bottom of exopher, respectively. YFP signal also forms a dim ring around mCherry spot. Lateral aspect shown, as in **a**. **h**, Thin sections (1–7, from 50 serial sections) through an exopher reveal a complex and heterogeneous structure. Additional membrane-bound objects at fringe of exopher main body (see panels 6, 7) may represent portions that have decayed from the original larger object, and are perhaps more easily phagocytosed by hypodermis, or shuttled along a tube for release into pseudocoelom. A small electron dense lysosome (L) lies beside exopher in panel 5. Scale bars, 2 μm (**a**, **c**, **e**, **g**), 1 μm (**d**, **f**, **h**).

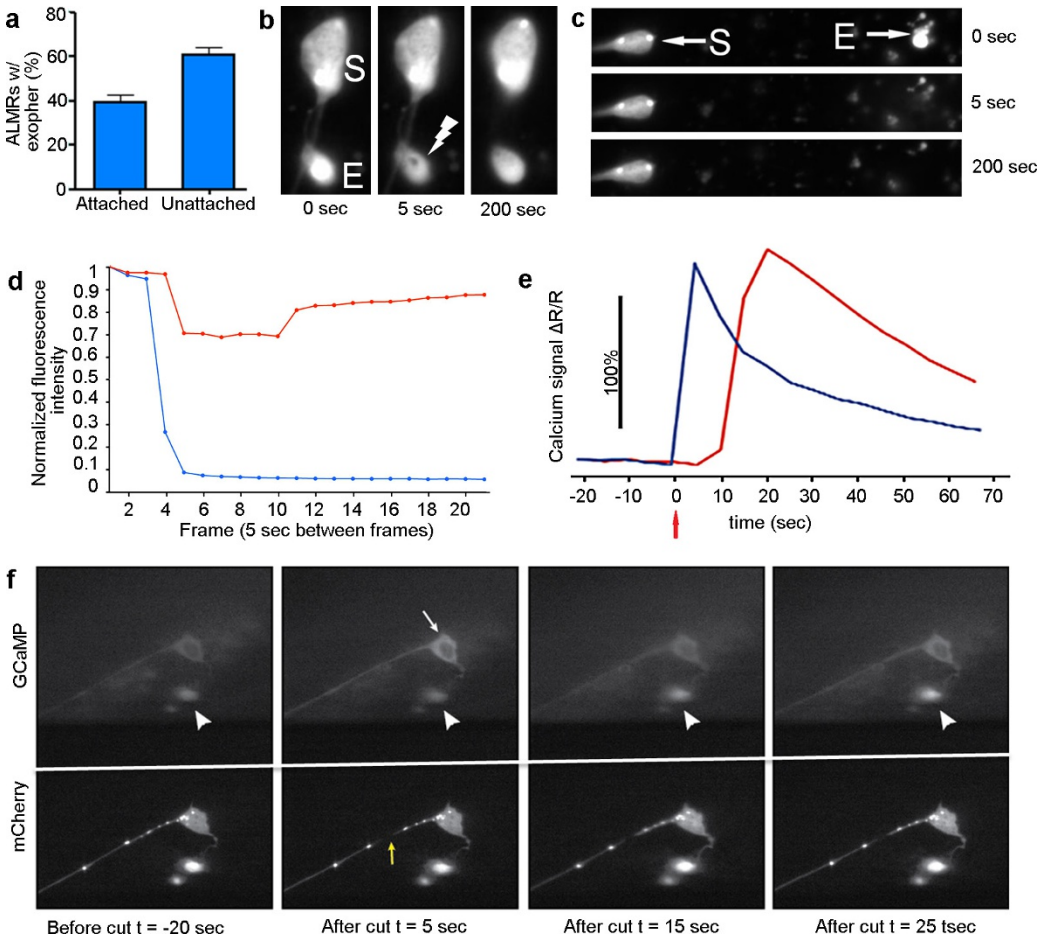

Extended Data Figure 3 | Fluorescence recovery after photo-bleaching (FRAP) and post-axotomy calcium imaging indicate that exophers that appear connected to the soma can fill with cytoplasmic materials. **a**, Both connected and unconnected exophers can be identified at high frequency in the same strain with a 40× objective. Strain is Is[$P_{mec\text{-}4}$ mCh1], adult day 2; $n = 77$ total, 3 trials. Data are mean ± s.e.m. **b**, Example of a connected ALMR exopher recovering after laser bleaching. Strain is Is[$P_{mec\text{-}4}$mCh1]; Is[$P_{mec\text{-}4}$GFP], adult day 2. Before laser treatment is '0 s', other times are post-treatment. **c**, Example of a detached ALMR exopher photo-bleaching and failing to refill. Strain is Is[$P_{mec\text{-}4}$mCh1]; Is[$P_{mec\text{-}4}$GFP], adult day 2. **d**, Fluorescence recovery measurements reveal that some connected exophers are able to transport fluorescent material from the cytoplasm to the exopher, whereas disconnected exophers do not appear to transport fluorescent material. Shown are data for examples in **b** (red, connected) and **c** (blue, unconnected) above. **e**, Time-lapse measurements of fluorescence intensity of the soma (blue trace) and the exopher (red trace) during the laser axotomy experiment in **f** show that the injury-induced calcium wave in the soma is followed by a pulse of calcium increase in the exopher (red arrow, laser axotomy at $t = 0$ s). We analysed two individual neurons with exophers connected to the soma and three individual neurons with what appeared to be non-connected exophers. Only the clearly connected exophers gave a calcium response comparable (~100% signal) to that measured at the cell soma as in this panel. Strain is ZB4059 *bzIs163*[$P_{mec\text{-}4}$::GCaMP3.0::SL2::mCherry]. **f**, The soma calcium wave induced by laser axotomy is followed by a calcium wave to connected exophers. We laser-cut an ALMR neuron that had a connected exopher in a day 2 adult that expressed both mCherry and the calcium-sensitive fluorophore, GCaMP3. We made the laser cut 20 μm along the axon (yellow arrow) at time $t = 0$, while taking simultaneous time-lapse images (1 frame per 5 s). Selected frames are shown at $t = -20$ s (before laser axotomy), right after laser axotomy at $t = 5$ s (note increased fluorescence in the soma; white arrow), and at $t = 15$ s and 25 s post-axotomy (note the later exopher increase in fluorescence; white arrowheads). Signal quantification is in **e**. Supplementary Video 3 shows the calcium wave that travels from soma to exopher.

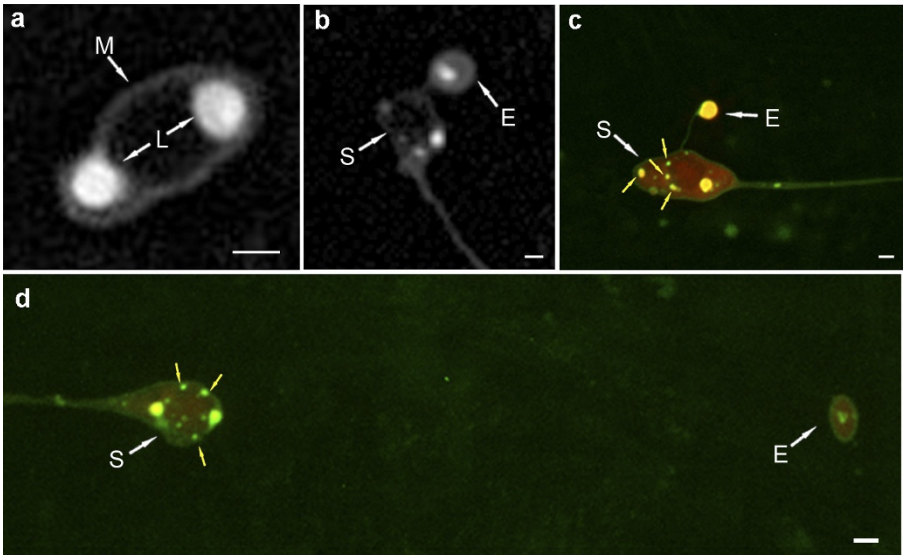

Extended Data Figure 4 | Lysosomes can be found in exophers. GFP-tagged lysosomes in touch neurons (*bzIs168*[P$_{mec\text{-}7}$LMP-1::GFP]) can be extruded in exophers in two types of lysosomal arrangements: (1) those that have small lysosome-like concentrated fluorescence, with mCherry dispersed (**d**), and (2) those that are nearly fully loaded with lysosome-like staining in which mCherry is also present throughout. **a**, Neuron soma featuring typical two large LMP-1::GFP-tagged pericentric lysosome domains, with no smaller ones evident. Strain is ZB4509 Is[P$_{mec\text{-}4}$mCh1]; *bzIs168*[P$_{mec\text{-}7}$LMP-1::GFP], green channel shown. As observed previously[43], the LMP-1::GFP signal clearly marks the plasma membrane (M), but less intensely than the lysosomes (L). **b**, LMP-1::GFP reveals lysosome inclusions are frequent and sometimes prominent in exophers. Strain is ZB4070 *bzIs168*[P$_{mec\text{-}7}$LMP-1::GFP]. We found that 18 out of 25 (72%) of exophers scored contained lysosomes in day 2 adults. Note that LMP-1::GFP faintly labels membrane[43] and rings the exopher in **b**–**d**, supporting that the exopher is membrane-bound. **c**, **d**, Co-labelling of aggregating mCherry and lysosome compartments suggests two types of lysosomal organization in exophers. Strain is ZB4509 Is[P$_{mec\text{-}4}$mCh1]; *bzIs168*[P$_{mec\text{-}7}$LMP-1::GFP]. **c**, Some exophers appear to be filled with LMP-1::GFP and coincident mCherry. **d**, LMP-1::GFP-tagged lysosomes included in exophers can be small and differentially localized from mCherry. In the absence of stress, neurons typically feature two large intensely fluorescent pericentric lysosome domains with LMP-1::GFP, with few smaller ones evident (see **a**). Neurons that had an exopher tended to also have additional small mobile lysosomes that we did not observe in cells without an exopher (see **b**–**d**). Additionally, neurons that featured 'large lysosome' exophers generally appeared to have fewer of the large perinuclear lysosomes in the soma (example in **d**). Scale bars, 2 μm. The inclusion of lysosomes in exophers suggests that some elimination of expelled material might be accomplished via internal degradation. Alternatively, dysfunctional lysosomes might be expelled via exophers.

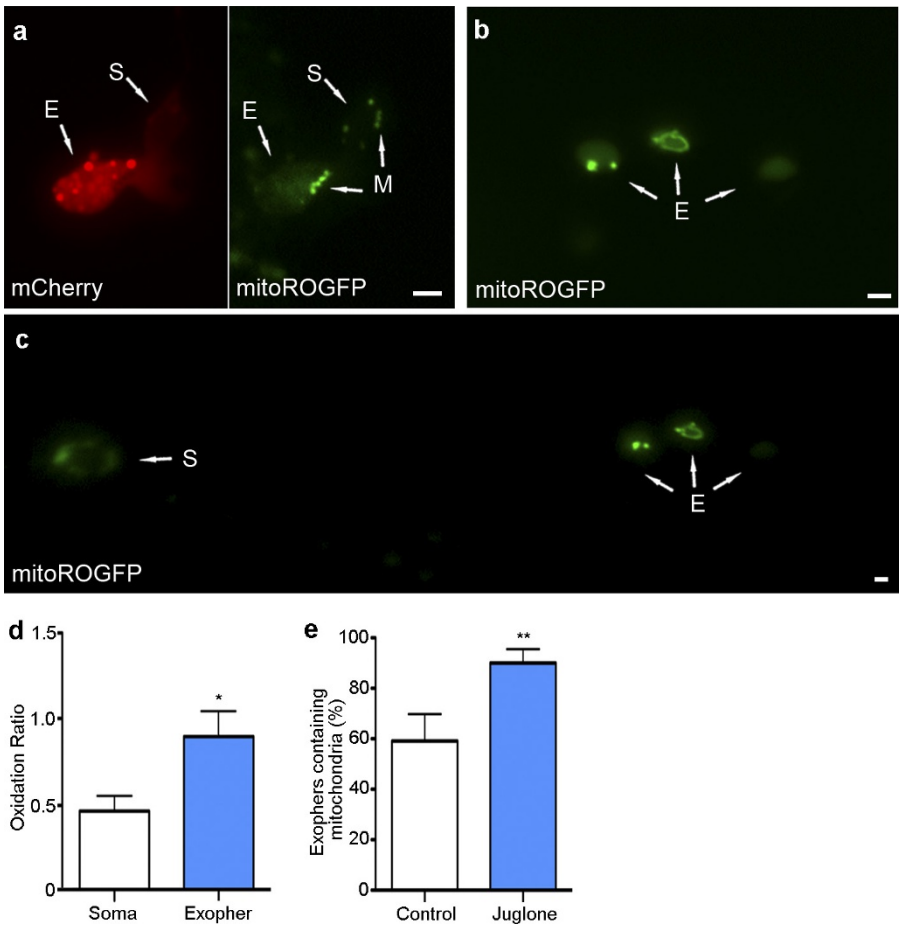

Extended Data Figure 5 | Mitochondria GFP markers exhibit a normal mitochondrial appearance in exophers. a, Mitochondria in exophers can form a network. Strain is Is[$P_{mec\text{-}4}$mitoLS::ROGFP]; Is[$P_{mec\text{-}4}$mCh1]). Shown is an exopher budding off from the ALMR soma. The exopher contains a disproportionate number of punctate mCherry aggregates, and also includes a GFP signal typical in size for neuronal mitochondria. The mitochondria in the exopher exhibit a filamentous structure similar to those in the soma, and the signal does not co-localize with the mCherry signal but may remain within a distinct sub-cellular domain. These two observations are consistent with the mitoGFP label localized to actual mitochondria as opposed to representing mislocalized GFP-labelled protein. **b**, Exophers can contain punctate mitochondria, networked mitochondria, or no mitochondria. Strain is Is[$P_{mec\text{-}4}$mitoLS::ROGFP]; Is[$P_{mec\text{-}4}$mCh1]). In the left exopher, the mitoROGFP signal is localized to two puncta. The middle exopher contains networked mitochondria. The right exopher contains no visible mitoROGFP signal. **c**, Zoomed out view of **b**, to show location of exophers relative to the touch neuron soma. Scale bars, 2 μm (**a**–**c**). **d**, MitoTimer fluorescent reporter reveals a difference in the mitochondrial matrix oxidation environment in exophers versus somas. We used a single-copy $P_{mec\text{-}4}$MitoTimer reporter to measure the relative red/green signal in exopher–soma pairs. Exophers have proportionately more oxidized signal, suggesting 'older' mitochondria (with more oxidation of the matrix-localized reporter) are preferentially expelled. $n = 7$ exophers, single exopher mean ± s.e.m. $^{*}P < 0.05$, paired *t*-test. **e**, Pharmacological disruption of mitochondria leads to higher rates of mitochondrial inclusion in exophers. Strain Is[$P_{mec\text{-}4}$mCh1]; *zhsEx17*[$P_{mec\text{-}4}$mitoLS::ROGFP] was treated with 230 μM juglone, which increases ROS production. Exophers from ALMR neurons exposed to juglone (blue, $n = 30$ total exophers) were significantly more likely to include at least one mitochondrion than untreated control exophers (white, $n = 22$ total exophers); 3 trials. Mitochondrial extrusion increases under conditions of juglone-induced oxidative stress. Data are mean ± s.e.m. $^{**}P < 0.01$, unpaired *t*-test.

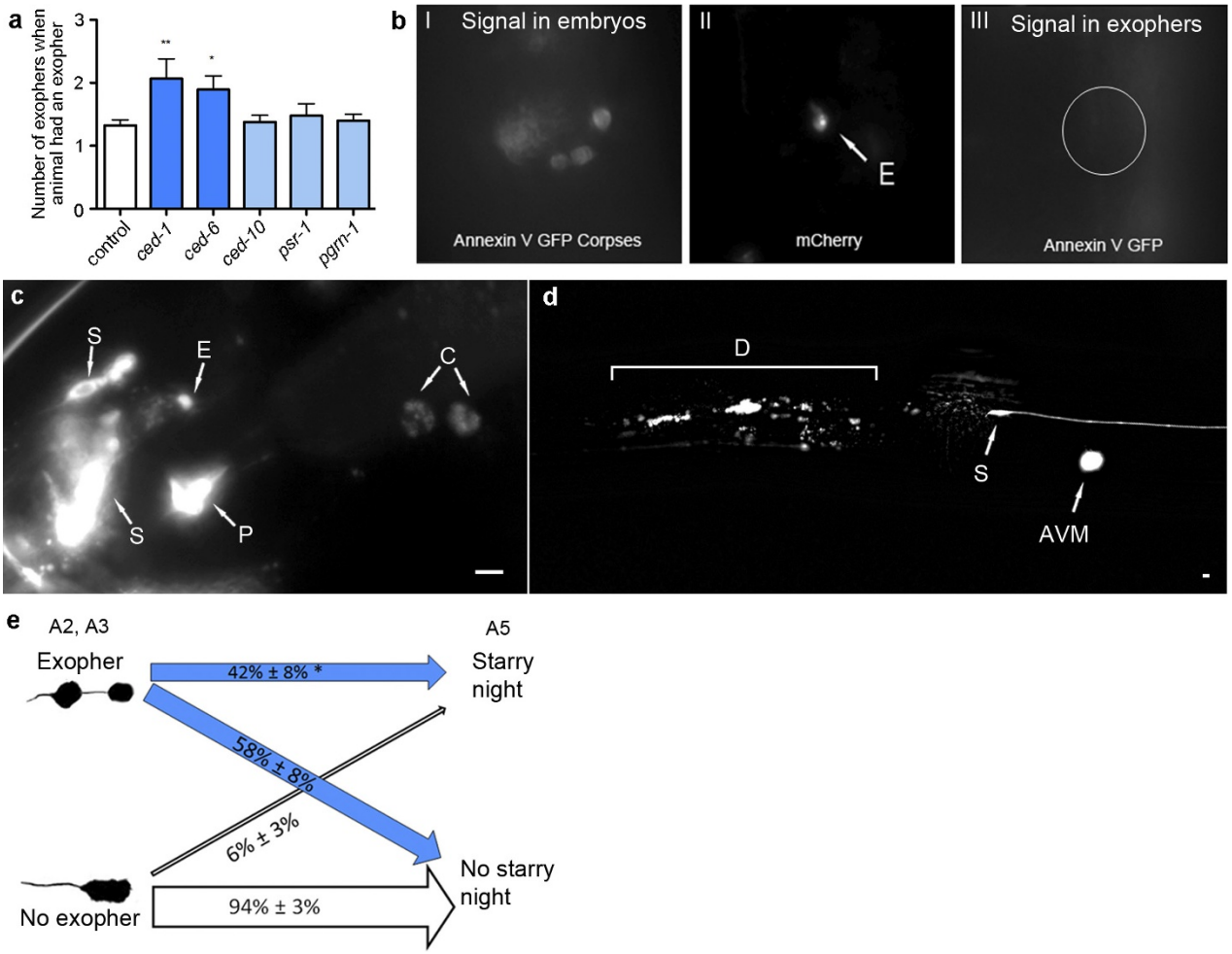

Extended Data Figure 6 | RNAi knockdown of *ced-1* and *ced-6*, but not other engulfment machinery, increases occurrence of mutiple exopher detection. a, RNAi knockdown of *ced-1* and *ced-6* engulfment genes increases the number of ALMR neurons with ≥2 exophers near the touch neurons, supporting conclusions from mutants. Control is empty vector, strain is ZB4071 *bzIs169*[$P_{mec\text{-}18}$*sid-1*$P_{sng\text{-}1}$YFP]; *bzIs101*[$P_{mec\text{-}4}$mCherry], at least 3 trials each, $n > 30$ ALMRs measured per trial; $n > 15$ cells with exopher per condition graphed. Data are mean ± s.e.m. $^{*}P < 0.05$, $^{**}P < 0.01$, one-way ANOVA with Dunnett's test. *ced-1* and *ced-6* RNAi do not increase the percentage of ALMRs that produce exophers (data not shown). **b**, Phosphatidylserine indicator annexinV::GFP (ref. 44) labels apoptotic corpses, but not mCherry-labelled exophers in strain ZB4083 *smIS76*[$P_{hsp\text{-}16}$ANV::GFP]; Is[$P_{mec\text{-}4}$mCh1]. Phosphatidylserine can be recognized on corpses of necrotic touch neurons, showing that touch neurons can produce surface phosphatidylserine and be recognized by annexinV-tagging, when inappropriately induced to die[33,44]. 0 out of 18 fluorescent mCherry-labelled exophers were co-labelled with annexinV::GFP. *ced-1* RNAi in the annexinV::GFP line did not improve phosphatidylserine detection on exophers ($n = 0$ out of 25 additional observations; not shown). **c**, In a DiI-soaked N2 animal, an amphid exopher originating from the ASIR soma can be seen proximal to the terminal bulb of the pharynx (P). The anterior coelomocytes ccAR and ccPR (C) also contain DiI, which must have been taken in and then jettisoned by the chemosensory amphid neurons and subsequently engulfed, analogously to the mCherry detected in Is[$P_{mec\text{-}4}$mCh1] coelomocytes. Thus, coelomocytes can scavenge the contents of exophers that are generated under normal physiological conditions, without the added stress of a potentially aggregating product of a transgene. Scale bar, 5 μm. **d**, In ZB4082 *cup-4(ok837);* Is[$P_{mec\text{-}4}$mCh1] mutants in which coelomocyte uptake is disrupted, an increased incidence of dispersed (D) fluorescence occurs (bracket denotes 'starry night phenotype', present in 29 out 200 animals, adult day 4). Similar dispersions are rare in *cup-4*(+) lines. Scale bar, 2 μm. AVM soma is also visible. **e**, Young adult animals that produced an exopher often later exhibit the starry night phenotype, suggesting that mCherry material can move through the body. Is[$P_{mec\text{-}4}$ mCh1] animals were separated into populations that had an ALMR exopher on adult days 2 or 3 (blue arrows), and a population that had no ALMR exopher on days 2 or 3 (white arrows). Animals were scored again on day 5 for presence of the starry night phenotype. In the exopher-producing and non-exopher-producing groups, 42% and 6%, respectively, of animals exhibited a starry night phenotype. $n = 60$ total per group, 3 trials. Data are mean ± s.e.m. $^{*}P < 0.05$, unpaired *t*-test. Arrow thickness is weighted according to relative incidence. Note differences are likely to be underestimated here, as the 'no exopher' category should include animals that have produced exophers, but were not present at the time of sampling.

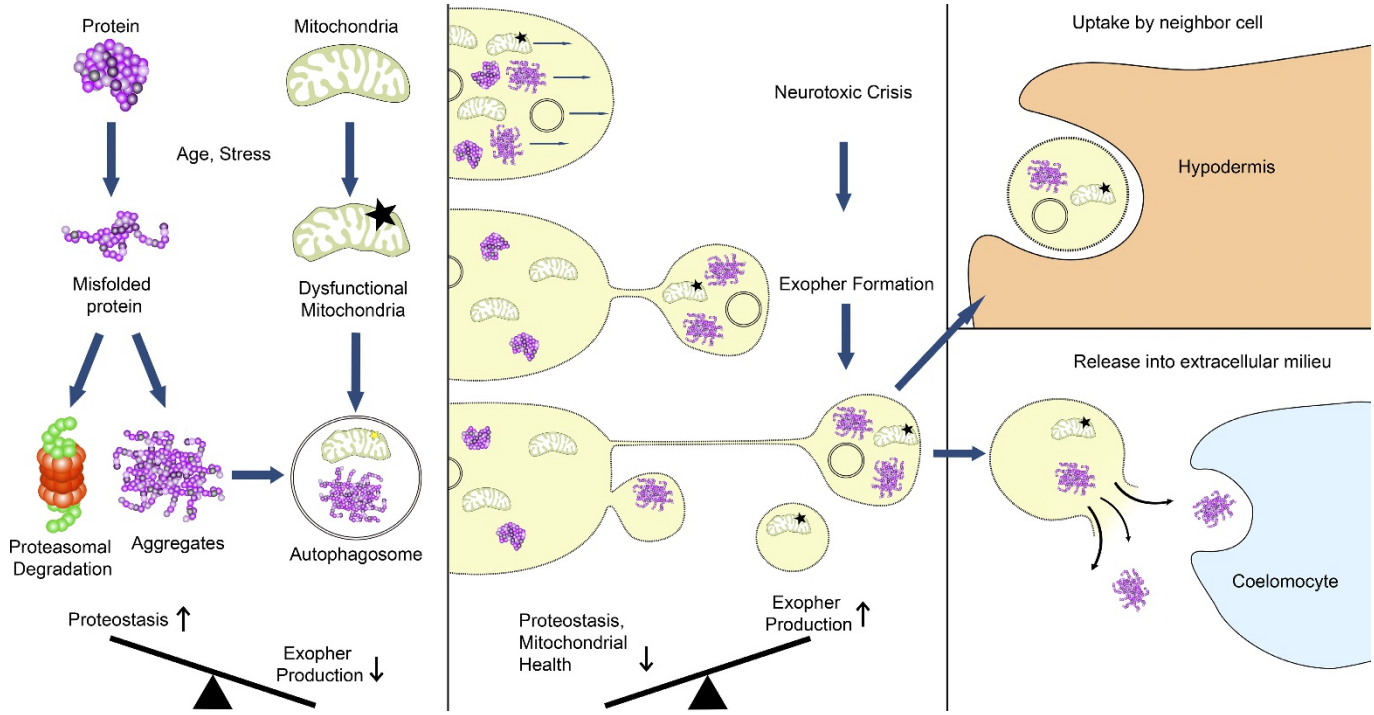

Extended Data Figure 7 | Working model for a proposed exopher role in proteostasis. As neurotoxic events such as protein aggregation or mitochondrial dysfunction occur in the cell, several homeostatic mechanisms clear them (left panel). At the young adult transition point to adult proteostasis (heat shock response down, unfolded protein response down, proteasome activity up[12–14]) or when basal levels of damage reach a threshold and overwhelm neuronal proteostasis, aggregates and organelles such as mitochondria and lysosomes are sequestered into a compartment that can be jettisoned from the cell. This compartment might include aggresomes described in mammalian cells[42]. For touch neurons, extruded exopher contents may be degraded by accompanying lysosomes, digested by the surrounding hypodermis, or may be re-extruded and reach the pseudocoelom to be taken up by coelomocytes. The process of exopher-genesis appears to be neuroprotective in young adults, but when dysregulated, might induce toxicity in neighbouring tissues. We speculate that exopher contents that cannot be degraded or passed on could remain in the neighbouring cell, where they could contribute to dysfunction. Exopher-genesis may be akin to the process by which protein aggregates and mitochondria become localized to neighbouring cells in humans, promoting the spread of disease.

Extended Data Table 1 | Effect of RNAi knockdown of genes functioning in exosome biogenesis and cell cycle progression on exopher detection

a. **Exosome Biogenesis**

Process Targeted	Gene Name	*P*-value
ESCRT-0	*hgrs-1*	0.48
	stam-1	0.21
ESCRT-1	*tsg-101*	0.55
	vps-28	0.67
	vps-37	0.22
ESCRT-2	*vps-22*	0.50
	vps-25	0.96
	vps-36	0.54
ESCRT-3	*vps-20*	0.49
	vps-24	0.89

b. **Cell Cycle-related**

Gene Name	*P*-value	Gene Name	*P*-value
cki-1	0.03*	*cit-1.2*	0.75
ccnk-1	0.46	*cki-2*	0.83
cdk-4	0.84	*cya-1*	0.52
cdk-9	0.68	*cya-2*	0.45
cdk-1	0.40	*cyb-2.1*	0.52
cdk-12	0.23	*cyd-1*	0.95
cdk-5	0.72	*cye-1*	0.95
cdk-8	0.79	*cyl-1*	0.32
cic-1	0.95	*dpl-1*	0.94

a, **b**, Neither ESCRT proteins required for exosome biogenesis nor cell cycle-related homologues exert major influences on exopher-genesis. **a**, RNAi knockdown of ESCRT genes did not significantly affect exopher occurrence. Strain is *bzIs169*[$P_{mec\text{-}18}$*sid-1* $P_{sng\text{-}1}$YFP]; *bzIs101*[$P_{mec\text{-}4}$mCherry; *unc-119*$^{+}$]; *hsf-1(sy441).* For each listed gene, the *P* value is from at least 3 trials, $n > 100$ total per condition, unpaired *t*-test. Note that negative results for RNAi screens are not definitive. The data support that the biogenesis of the exopher is distinct from the biogenesis of exosomes (see also Extended Data Table 2). **b**, RNAi knockdown of homologues of cell cycle-related genes did not significantly influence exopher production, with the exception of *cki-1*. Reducing *cki-1* activity by RNAi causes extra larval cell divisions[45], so its inhibition of exopher-genesis, although interesting, is not consistent with new cell division underlying exopher production. Note that *cdk-4* and *cyd-1* are required for cell cycle progression in postembryonic cells. Strain is *bzIs169*[$P_{mec\text{-}18}$*sid-1* $P_{sng\text{-}1}$YFP]; *bzIs101*[$P_{mec\text{-}4}$mCherry; *unc-119*$^{+}$]. For each listed gene, the *P* value is from at least 3 trials, $n > 100$ total per condition, unpaired *t*-test. False discovery rate (FDR) statistic for *cki-1* RNAi is $q = 0.04$, Benjamini–Hochberg FDR calculator.

Extended Data Table 2 | Comparison of features of exophers to other characterized extracellular vesicles

	Exosomes	Microvesicles	Migrasomes	Exophers
Diameter	30 nm–100 nm[46]	100 nm–1,000 nm[46]	500 nm–3,000 nm[49]	1,000 nm–7,800 nm
Timing of release	Tens of minutes[47]	Seconds[47]	40–200 minutes[49]	15–60 minutes
Mechanism of Release	Multi-vesicular bodies fuse to the cell membrane[46]	Outward budding and scission[46]	Expands at tip of retraction fibers[49]	Jettisoned from cell body
ESCRT Machinery involved	Yes[47]	ESCRT3; *tsg-101*[47]	Unknown	No
Attachment to releasing cell	No	No	Yes (via retraction fibers)[49]	Sometimes (via thin fiber)
Actin required	No	No	Yes[49]	Yes
Vesicular Contents	DNA, RNA, Proteins, Lipids[46]	DNA, RNA, Proteins, Lipids[46]	Cytosol, Proteins[49]	Mitochondria, Lysosomes, Protein Aggregates
Phosphatidyl-serine Distribution	Membrane outer leaflet[46]	Membrane outer leaflet[48]	Unknown	Not displayed on membrane outer leaflet

References 46–49 are cited in this table.